Efficient discovery of potently neutralizing SARS-CoV-2 antibodies using LIBRA-seq with ligand blocking

Andrea R. Shiakolas[1,2], Nicole Johnson[3], Kevin J. Kramer[1,2], Naveenchandra Suryadevara[1], Daniel Wrapp[3], Sivakumar Periasamy[4,6], Kelsey A. Pilewski[1,2], Nagarajan Raju[1,2], Rachel Nargi[1], Rachel E. Sutton[1], Lauren Walker[1,2], James E. Crowe Jr[1,2,7], Alexander Bukreyev[4,5,6], Robert H. Carnahan[1,7], Jason S. McLellan[3], Ivelin S. Georgiev[1,2,8,9,10,11,12,*]

[1]Vanderbilt Vaccine Center, Vanderbilt University Medical Center, Nashville, TN, 37232, USA

[2]Department of Pathology, Microbiology, and Immunology, Vanderbilt University Medical Center, Nashville, TN, 37232, USA

[3]Department of Molecular Biosciences, The University of Texas at Austin, Austin, TX, 78712, USA

[4]Department of Pathology, University of Texas Medical Branch at Galveston, Galveston TX 77555, USA

[5]Department of Microbiology and Immunology, University of Texas Medical Branch at Galveston, Galveston TX 77555, USA

[6]Galveston National Laboratory, University of Texas Medical Branch at Galveston, Galveston TX 77555, USA

[7]Department of Pediatrics, Vanderbilt University Medical Center, Nashville, TN, 37232, USA

[8]Vanderbilt Institute for Infection, Immunology, and Inflammation, Vanderbilt University Medical Center, Nashville, TN, 37232, USA

[9]Department of Electrical Engineering and Computer Science, Vanderbilt University, Nashville, TN, 37232, USA

[10]Center for Structural Biology, Vanderbilt University, Nashville, TN, 37232, USA

26 [11]Program in Computational Microbiology and Immunology, Vanderbilt University Medical
27 Center, Nashville, TN, 37232, USA
28 [12]Lead Contact
29 *Corresponding author: ivelin.georgiev@vanderbilt.edu

30

31

32

33

34

ABSTRACT

SARS-CoV-2 therapeutic antibody discovery efforts have met with notable success but have been associated with a generally inefficient process, requiring the production and characterization of exceptionally large numbers of candidates for the identification of a small set of leads. Here, we show that incorporating antibody–ligand blocking as part of LIBRA-seq, the high-throughput sequencing platform for antibody discovery, results in efficient identification of ultra-potent neutralizing antibodies against SARS-CoV-2. LIBRA-seq with ligand blocking is a general platform for functional antibody discovery targeting the disruption of antigen–ligand interactions.

46 Technologies for developing preventive and therapeutic measures that can counteract
47 potential pandemics are of utmost significance for public health. The ongoing COVID-19
48 pandemic, for example, has emphasized the importance of developing effective
49 countermeasures quickly. Through various pandemic preparedness initiatives, effective SARS-
50 CoV-2-neutralizing antibodies were discovered and validated within months[1-7], as were SARS-
51 CoV-2 vaccine candidates[8]. However, even with such unprecedented speed of vaccine and
52 therapeutic development, the pandemic has inflicted devastating worldwide effects, including
53 the loss of millions of human lives, a long-lasting burden on the healthcare system, and
54 economic turmoil. Accelerating actions by several weeks or months can make an enormous
55 difference in an exponentially evolving pandemic, especially at the early stages of infection
56 spread. Therefore, the efficient discovery of effective countermeasures against emerging
57 pathogens can play a critical role in pandemic preparedness for future infectious disease
58 outbreaks.
59 Antibodies are a major modality for therapy against a wide range of diseases, including
60 infectious diseases, cancer, autoimmunity, cardiovascular, hematologic, neurologic diseases,
61 and others. Antibody discovery efforts have relied on a broad range of technologies, such as
62 hybridoma generation, antigen-specific B cell sorting, phage or yeast display, single-cell B cell
63 sequencing and others[9-14]. Overall, these efforts aim to identify paired heavy–light chain
64 antibody sequences isolated from human or animal samples with prior antigen exposure,
65 followed by monoclonal antibody production and functional characterization. However, with
66 these approaches for antibody discovery, limited information is typically obtained about the
67 antigen specificity of antibody candidates at the screening step. The recent development of the
68 LIBRA-seq (linking B cell receptor to antigen specificity through sequencing) technology enables
69 the simultaneous mapping of antibody sequence to antigen specificity for a large number of
70 antigens in a single next-generation sequencing experiment[15]. LIBRA-seq uses DNA-barcoded
71 antigens to transform B cell receptor (BCR)-antigen binding into a sequence-able event and is

72 of unique utility for discovering broadly reactive antibodies for pathogens that exhibit substantial
73 antigen variability. LIBRA-seq has been applied successfully to identify broadly reactive
74 antibodies against HIV-1, influenza viruses, and coronaviruses[15, 16].

75 Although using antigen binding alone as a readout can result in the successful
76 identification of functional antibodies, the discovery process can be inefficient, requiring time-
77 intensive subsequent monoclonal antibody validation steps. This limitation was exemplified by
78 the SARS-CoV-2 antibody discovery initiatives over the past year. Although these efforts have
79 met with notable success, resulting in numerous antibodies and antibody cocktails in clinical
80 trials or approved for emergency use[17-19], testing of large numbers of antibodies (frequently
81 hundreds to thousands) was generally required. Typically, a small fraction of tested antibodies
82 was neutralizing, with hit rates in the range of 0.3 to 23% in various studies[2-7].

83 To overcome this limitation, we developed LIBRA-seq with ligand blocking, a second-
84 generation LIBRA-seq technology that incorporates a functional readout into the antibody
85 discovery process. To achieve this goal, a ligand and its cognate target antigen(s) are each
86 labeled with a unique oligonucleotide barcode (**Supplementary Figure 1A**), enabling the
87 transformation of antigen-ligand interactions into sequence-able events. This allows for the
88 identification of B cells that have high LIBRA-seq scores for the target antigen(s) and low
89 LIBRA-seq scores for the ligand, as B cells that are likely able to potently block antigen-ligand
90 interactions (**Supplementary Figure 1A**). Therefore, a single high-throughput LIBRA-seq with
91 ligand blocking experiment provides both binding (antigen recognition) and functional (ligand
92 blocking) information for thousands of B cells at a time, at the single-cell level.

93 As a proof of concept, we performed antibody discovery for SARS-CoV-2-specific
94 antibodies from the peripheral B cells from convalescent subjects with past SARS-CoV-2
95 infection. This provides a suitable opportunity for validating the LIBRA-seq with ligand blocking
96 technology since antibodies that block the interactions of the SARS-CoV-2 spike (S) protein with
97 its receptor angiotensin-converting enzyme 2 (ACE2) are among the most potently neutralizing

98 identified to date[2-7, 17-19]. We performed three separate LIBRA-seq experiments, with screening
99 libraries that included: experiment 1, ACE2 and SARS-CoV-2 S; experiment 2, a titration series
100 of different aliquots of SARS-CoV-2 S, each labeled with a unique barcode; and experiment 3,
101 ACE2 and a titration series of S (**Figure 1A**). The incorporation of a titration series of the S
102 antigen in the LIBRA-seq screening library for experiments 2 and 3 aimed to assess the
103 strength of BCR-antigen interactions through a sequencing readout (**Supplementary Figure**
104 **1B, C**). The antigen screening library for each of the experiments also included an influenza
105 virus hemagglutinin and an HIV-1 envelope variant protein as controls.
106 The application of LIBRA-seq resulted in 829, 830, and 957 antigen-specific B cells for
107 the three experiments, respectively. We prioritized a set of B cells for monoclonal antibody
108 production and validation based on the following conditions: for experiments 1 and 3 where
109 ACE2 was included in the screening library, we selected B cells with high LIBRA-seq scores for
110 S and low scores for ACE2; and for experiment 2, we selected B cells that had positive scores
111 for multiple aliquots of S (**Figure 1B-D**). B cells with high S and high ACE2 LIBRA-seq scores
112 were also selected as controls from experiments 1 and 3, along with an influenza-specific B cell
113 from experiment 2 (**Figure 1B-D**). Although some of the selected antibodies appeared to be
114 clonally related, overall they exhibited diverse sequence features, including V_H- and J_H-gene
115 usage, HCDR3 lengths, and somatic mutation numbers for both the heavy and light chains
116 (**Supplementary Figure 2A**).
117 To confirm the predicted antigen specificity for the selected antibodies, we tested them
118 for binding to S ectodomain by ELISA (**Figure 2A, Supplementary Figure 2B**). The LIBRA-seq
119 predicted antigen specificity was confirmed for 26 of 27 (96%) antibodies, including 25 SARS-
120 CoV-2 antibodies and 1 influenza virus antibody. Next, to map the general antibody epitope
121 regions, we also tested the antibodies for binding to S1, S2, receptor-binding domain (RBD),
122 and N-terminal domain (NTD) proteins (**Figure 2A, Supplementary Figure 2B**). The majority of
123 the antibodies from experiments 1 and 3 recognized the RBD, whereas none of the antibodies

124 from experiment 2 recognized the RBD, suggesting that the inclusion of a sequencing readout
125 for ACE2 blocking impacted the ability to select antibodies with target epitope specificities
126 (**Figure 2A, Supplementary Figure 2B**). The antibodies had a wide range of affinities for RBD
127 or NTD, including several ultra-potent antibodies (K_D <1 nM) from experiments 1 and 3 (**Figure**
128 **2B**). Next, we tested the ability of the antibodies to block ACE2 binding to spike. For the
129 antibodies predicted to block ACE2 by LIBRA-seq, 57% from experiment 1 and 67% from
130 experiment 3 demonstrated ACE2 blocking ability via ELISA (**Figure 2C, Supplementary**
131 **Figure 2C**). In contrast, no antibodies from experiment 2 blocked ACE2 binding (**Figure 2C,**
132 **Supplementary Figure 2C**). In addition, we tested the antibodies in a VSV SARS-CoV-2
133 chimeric virus neutralization assay. For the antibodies predicted to block ACE2 by LIBRA-seq,
134 86% from experiment 1 and 67% from experiment 3 were neutralizing (**Figure 2D-F**). In
135 contrast, only two clonally related antibodies (25%) from experiment 2 were neutralizing (**Figure**
136 **2D-F, Supplementary Figure 2D**). These results highlight the importance of including ligand
137 blocking in the LIBRA-seq screening for selectively identifying potently neutralizing antibodies.
138 Significant differences were not detected for the neutralization potencies between antibodies
139 from experiments 1 and 3 (p-value: >0.99, ANOVA with the Kruskal-Wallis Test; **Figure 2E**),
140 suggesting that antigen titrations did not have a significant effect on the ability to identify
141 potently neutralizing antibodies.
142 Next, we tested a panel of antibodies for neutralization of authentic SARS-CoV-2 virus in
143 a plaque reduction neutralization test and found that, just as in the VSV assay, antibody 5317-4
144 exhibited the most potent neutralization, with an IC_{50} value of 7.3 ng/mL (**Figure 2G**), on par
145 with antibodies currently in clinical trials or approved for emergency use[17-19]. In addition, to
146 investigate the recognition of SARS-CoV-2 S by LIBRA-seq-identified antibodies, we
147 determined a 9 Å-resolution Cryo-EM structure of the antigen-binding fragments (Fabs) of 5317-
148 4 and another neutralizing antibody, 5317-10, bound to the SARS-CoV-2 S extracellular domain
149 (ECD) (**Figure 2H**). We chose 5317-4 based on its potent neutralization, high affinity for the S

150 RBD, and ACE2 competition. The 3D reconstruction revealed that 5317-4 binds to the RBD in
151 the “up” and “down” conformations, and its epitope partially overlaps the ACE2 binding footprint
152 (**Figure 2H-I**). In the RBD up position, 5317-4 binds near the receptor-binding motif at an angle
153 that appears to moderately clash with RBD-bound ACE2 (**Figure 2I**). Additionally, when bound
154 to the RBD in the down conformation, 5317-4 competes with ACE2 binding to the adjacent,
155 otherwise accessible RBD in the up position (**Figure 2I**). 5317-10 was of interest due to its
156 inconclusive epitope bin, as it bound to S1, but not to the individual RBD or NTD constructs
157 (**Figure 2A**). The map revealed that 5317-10 binds a novel quaternary epitope that bridges an
158 RBD in the down position and the NTD of an adjacent protomer (**Figure 2H**). This mode of
159 recognition may prevent the RBD from transitioning into an ACE2-accessible up position,
160 thereby preventing binding by ACE2.

161 Together, the results from the three LIBRA-seq experiments showcase the advantages
162 of including ligand blocking as part of the sequencing readout. The experiment without ligand
163 blocking (experiment 2) had a lower hit rate for identifying virus-neutralizing antibodies. Through
164 a single high-throughput sequencing experiment, LIBRA-seq with ligand blocking identified ultra-
165 potent SARS-CoV-2 antibodies, requiring the subsequent production and validation of less than
166 a dozen antibodies per experiment. The observed hit rates for the discovery of potently
167 neutralizing antibodies are a substantial improvement over what has been reported in the
168 literature, which typically required the screening of hundreds to thousands of antibody
169 candidates to identify a small number of antibodies with similar levels of neutralization potencies
170 to the antibodies described in this manuscript[2-7]. The ability to save weeks or months during the
171 antibody lead discovery process can have an extraordinary impact on the evolution of an
172 infectious disease outbreak, especially in the early stages of infection spread. As such, the
173 application of LIBRA-seq with ligand blocking for the efficient discovery of highly potent
174 antibodies can provide critical advantages for rapid development of therapeutic and preventive
175 countermeasures. More broadly, LIBRA-seq with ligand blocking presents a general platform for

176 discovering functional antibodies, with applications to virtually any area where targeting the
177 disruption of antigen-ligand interaction is a prime therapeutic goal.
178

179 **Acknowledgements**

180 We thank Angela Jones, Latha Raju, and Jamie Roberson of Vanderbilt Technologies for
181 Advanced Genomics for their expertise regarding NGS and library preparation; David Flaherty
182 and Brittany Matlock of the Vanderbilt Flow Cytometry Shared Resource for help with flow panel
183 optimization; and members of the Georgiev laboratory for comments on the manuscript. The
184 Vanderbilt VANTAGE Core provided technical assistance for this work. VANTAGE is supported
185 in part by CTSA grant 5UL1 RR024975-03, the Vanderbilt Ingram Cancer Center (P30
186 CA68485), the Vanderbilt Vision Center (P30 EY08126), and NIH/NCRR (G20 RR030956). This
187 work was conducted in part using the resources of the Advanced Computing Center for
188 Research and Education at Vanderbilt University (Nashville, TN). Flow cytometry experiments
189 were performed in the VUMC Flow Cytometry Shared Resource. The VUMC Flow Cytometry
190 Shared Resource is supported by the Vanderbilt Ingram Cancer Center (P30 CA68485) and the
191 Vanderbilt Digestive Disease Research Center (DK058404).

192 For work described in this manuscript, I.S.G., A.R.S., K.J.K., K.A.P., N.R., and L.W. were
193 supported in part by NIH NIAID award R01AI131722-S1, the Hays Foundation COVID-19
194 Research Fund, Fast Grants, and CTSA award No. *UL1 TR002243* from the National Center for
195 Advancing Translational Sciences. J.S.M, N.J., and D.W. were supported in part by a National
196 Institutes of Health (NIH)/National Institute of Allergy and Infectious Diseases (NIAID) grant
197 awarded to J.S.M. (R01-AI127521), Welch Foundation grant F-0003-19620604, and NIH NIAID
198 award R01AI131722-S1. This work was supported by Defense Advanced Research Projects
199 Agency (DARPA) grant HR0011-18-2-0001, U.S. N.I.H. contract 75N93019C00074, N.I.H. grant
200 R01 AI157155, the Dolly Parton COVID-19 Research Fund at Vanderbilt, and a grant from Fast

Grants, Mercatus Center, George Mason University. J.E.C. is a recipient of the 2019 Future Insight Prize from Merck KGaA, which supported this work with a grant.

Author Contributions

Methodology, A.R.S. and I.S.G.; Investigation, A.R.S., N.J., K.J.K., N.S., D.W., S.P., K.A.P., N.J., R.N., R.E.S., L.W., J.E.C., A.B., R.H.C., J.S.M., and I.S.G.; Software, A.R.S., N.R.; Validation, A.R.S., K.J.K.; Writing - Original Draft, A.R.S. and I.S.G.; Writing -Review & Editing, all authors; Funding Acquisition, I.S.G., J.E.C., A.B., R.H.C., J.S.M., and A.R.S, and K.J.K.; Resources, I.S.G., J.E.C., A.B., R.H.C., and J.S.M..; Supervision, I.S.G.

Declaration of Interest

A.R.S. and I.S.G. are co-founders of AbSeek Bio. I.S.G., A.R.S, and K.J.K. are listed as inventors on antibodies described herein. J.E.C. has served as a consultant for Luna Biologics, is a member of the Scientific Advisory Board Meissa Vaccines and is Founder of IDBiologics. The Crowe laboratory has received funding support in sponsored research agreements from AstraZeneca, IDBiologics, and Takeda. The Georgiev laboratory at Vanderbilt University Medical Center has received unrelated funding from Takeda Pharmaceuticals.

METHODS

Donor Information

PBMC samples were purchased from Cellero. The PBMCs were from subjects with past SARS-CoV-2 infection at least 14 days post symptom cessation. For experiment 1, three samples were pooled from donors 523, 527, and 528. For experiments 2 and 3, samples from donor 523 were used for LIBRA-seq. Donor 523 had a plaque reduction neutralization test titer of 1:2,560.

227 **Antigen Purification**

228 A variety of recombinant soluble protein antigens were used in the LIBRA-seq experiment and
229 other experimental assays.

230 Plasmids encoding residues 1–1208 of the SARS-CoV-2 spike with a mutated S1/S2
231 cleavage site, proline substitutions at positions 817, 892, 899, 942, 986 and 987, and a C-
232 terminal T4-fibritin trimerization motif, an 8x HisTag, and a TwinStrepTag (SARS-CoV-2 spike
233 HP); 1−615 of human ACE2 with a C-terminal HRV3C protease cleavage site, a TwinStrepTag
234 and an 8XhisTag (ACE2) were transiently transfected in Expi293F cells using polyethylenimine.
235 Transfected supernatants were harvested 5 days after expression and purified over a StrepTrap
236 column (Cytiva Life Sciences), as previously described. Both recombinant SARS-CoV-2 S HP
237 and ACE2 were further purified to homogeneity using a Superose6 Increase column (Cytiva Life
238 Sciences).

239 For the HIV-1 gp140 SOSIP variant from strain ZM197 (clade C) and hemagglutinin from
240 strain A/New Caledonia/20/99 (H1N1) (GenBank ACF41878), recombinant, soluble antigens
241 contained an AviTag and were expressed in Expi293F cells using polyethylenimine transfection
242 reagent and cultured. FreeStyle F17 expression medium supplemented with pluronic acid and
243 glutamine was used. The cells were cultured at 37°C with 8% CO_2 saturation and shaking. After
244 5-7 days, cultures were centrifuged and supernatant was filtered and run over an affinity column
245 of agarose-bound *Galanthus nivalis* lectin. The column was washed with PBS and antigens
246 were eluted with 30 mL of 1M methyl-a-D-mannopyranoside. Protein elutions were buffer
247 exchanged into PBS, concentrated, and run on a Superdex 200 Increase 10/300 GL Sizing
248 column on the AKTA FPLC system. Fractions corresponding to correctly folded protein were
249 collected, analyzed by SDS-PAGE and antigenicity was characterized by ELISA using known
250 monoclonal antibodies specific to each antigen. AviTagged antigens were biotinylated using
251 BirA biotin ligase (Avidity LLC).

252 SARS-CoV-2 S1, SARS-CoV-2 S2, SARS-CoV-2 RBD and SARS-CoV-2 NTD proteins
253 were purchased from the commercial vendor, Sino Biological.
254
255 **DNA-barcoding of Antigens**
256 We used oligos that possess 15 bp antigen barcode, a sequence capable of annealing to the
257 template switch oligo that is part of the 10X bead-delivered oligos and contain truncated TruSeq
258 small RNA read 1 sequences in the following structure: 5′-
259 CCTTGGCACCCGAGAATTCCANNNNNNNNNNNNNNCCCATATAAGA*A*A-3′, where Ns
260 represent the antigen barcode as previously described[15]. For each antigen, a unique DNA
261 barcode was directly conjugated to the antigen itself. In particular, 5′ amino-oligonucleotides
262 were conjugated directly to each antigen using the SoluLINK Protein-Oligonucleotide
263 Conjugation Kit (TriLink cat no. S-9011) according to manufacturer's instructions. Briefly, the
264 oligo and protein were desalted, and then the amino-oligo was modified with the 4FB
265 crosslinker, and the biotinylated antigen protein was modified with S-HyNic. Then, the 4FB-oligo
266 and the HyNic-antigen were mixed. This process causes a stable bond to form between the
267 protein and the oligonucleotide. The concentration of the antigen-oligo conjugates was
268 determined by a BCA assay, and the HyNic molar substitution ratio of the antigen-oligo
269 conjugates was analyzed using the NanoDrop according to the SoluLINK protocol guidelines.
270 AKTA FPLC was used to remove excess oligonucleotide from the protein-oligo conjugates,
271 which were also verified using SDS-PAGE with a silver stain. Antigen-oligo conjugates were
272 also used in flow cytometric titration experiments.
273
274 **Antigen-specific B Cell Sorting**
275 Cells were stained and mixed with DNA-barcoded antigens and other antibodies, and then
276 sorted using fluorescence activated cell sorting (FACS). First, cells were counted, and viability

277 was assessed using trypan blue. Then, cells were washed three times with DPBS
278 supplemented with 0.1% bovine serum albumin (BSA). Cells were resuspended in DPBS-BSA
279 and stained with cell markers including viability dye (Ghost Red 780), CD14-APC-Cy7, CD3-
280 FITC, CD19-BV711, and IgG-PE-Cy5. Additionally, antigen-oligo conjugates were added to the
281 stain. After staining in the dark for 30 minutes at room temperature, cells were washed three
282 times with DPBS-BSA at 300 x g for five minutes. Cells were then incubated for 15 minutes at
283 room temperature with Streptavidin-PE to label cells with bound antigen. Cells were washed
284 three times with DPBS-BSA, resuspended in DPBS, and sorted by FACS. Antigen positive cells
285 were bulk sorted and delivered to the Vanderbilt Technologies for Advanced Genomics
286 (VANTAGE) sequencing core at an appropriate target concentration for 10X Genomics library
287 preparation and subsequent sequencing. Flow cytometry data were analyzed using FlowJo.
288

289 **Sample Preparation, Library Preparation, and Sequencing**

290 Single-cell suspensions were loaded onto the Chromium Controller microfluidics device (10X
291 Genomics) and processed using the B-cell Single Cell V(D)J solution according to
292 manufacturer's suggestions for a target capture of 10,000-20,000 B cells, with minor
293 modifications to intercept, amplify and purify the antigen barcode libraries as previously
294 described[15].
295

296 **Sequence processing and bioinformatic analysis**

297 We used our previously described pipeline to use paired-end FASTQ files of oligo libraries as
298 input, process and annotate reads for cell barcode, UMI, and antigen barcode, and generate a
299 cell barcode - antigen barcode UMI count matrix[15, 16]. BCR contigs were processed using Cell
300 Ranger (10X Genomics) using GRCh38 as reference. Antigen barcode libraries were also
301 processed using Cell Ranger (10X Genomics). The overlapping cell barcodes between the two
302 libraries were used as the basis of the subsequent analysis. We removed cell barcodes that had

303 only non-functional heavy chain sequences as well as cells with multiple functional heavy chain
304 sequences and/or multiple functional light chain sequences, reasoning that these may be
305 multiplets. Additionally, we aligned the BCR contigs (filtered_contigs.fasta file output by Cell
306 Ranger, 10X Genomics) to IMGT reference genes using HighV-Quest[20]. The output of HighV-
307 Quest was parsed using ChangeO[21] and merged with an antigen barcode UMI count matrix.
308 Finally, we determined the LIBRA-seq score for each antigen in the library by calculating the
309 centered-log ratios (CLR) of each antigen UMI count for each cell as previously described[15].
310

311 **Antibody Expression and Purification**

312 For each antibody, variable genes were inserted into custom plasmids encoding the constant
313 region for the IgG1 heavy chain as well as respective lambda and kappa light chains (pTwist
314 CMV BetaGlobin WPRE Neo vector, Twist Bioscience). Antibodies were expressed in Expi293F
315 mammalian cells (Thermo Fisher Scientific) by co-transfecting heavy chain and light chain
316 expressing plasmids using polyethylenimine transfection reagent and cultured for 5 to 7 days.
317 Cells were maintained in FreeStyle F17 expression medium supplemented at final
318 concentrations of 0.1% Pluronic Acid F-68 and 20% 4 mM L-Glutamine. These cells were
319 cultured at 37°C with 8% CO_2 saturation and shaking. After transfection and 5-7 days of culture,
320 cell cultures were centrifuged and supernatant was 0.45 µm filtered with Nalgene Rapid Flow
321 Disposable Filter Units with PES membrane. Filtered supernatant was run over a column
322 containing Protein A agarose resin equilibrated with PBS. The column was washed with PBS,
323 and then antibodies were eluted with 100 mM Glycine HCl at 2.7 pH directly into a 1:10 volume
324 of 1M Tris-HCl pH 8.0. Eluted antibodies were buffer exchanged into PBS 3 times using Amicon
325 Ultra-centrifugal filter units and concentrated. Antibody plasmids were sequenced. If antibody
326 sequences did not match expected heavy or light chain, antibody was excluded from
327 downstream analysis.
328

329 **High-throughput Antibody Expression**

330 For high-throughput production of recombinant antibodies, approaches were used that are
331 designated as microscale. For antibody expression, microscale transfection was performed
332 (~1 mL per antibody) of CHO cell cultures using the Gibco ExpiCHO Expression System and a
333 protocol for deep 96-well blocks (Thermo Fisher Scientific). In brief, synthesized antibody-
334 encoding DNA (~2 µg per transfection) was added to OptiPro serum free medium (OptiPro
335 SFM), incubated with ExpiFectamine CHO Reagent and added to 800 µL of ExpiCHO cell
336 cultures into 96-deep-well blocks using a ViaFlo 384 liquid handler (Integra Biosciences). The
337 plates were incubated on an orbital shaker at 1,000 r.p.m. with an orbital diameter of 3 mm at
338 37°C in 8% CO_2. The next day after transfection, ExpiFectamine CHO Enhancer and ExpiCHO
339 Feed reagents (Thermo Fisher Scientific) were added to the cells, followed by 4 d incubation for
340 a total of 5 d at 37°C in 8% CO_2. Culture supernatants were collected after centrifuging the
341 blocks at 450 x *g* for 5 min and were stored at 4°C until use. For high-throughput microscale
342 antibody purification, fritted deep-well plates were used containing 25 µL of settled protein G
343 resin (GE Healthcare Life Sciences) per well. Clarified culture supernatants were incubated with
344 protein G resin for antibody capturing, washed with PBS using a 96-well plate manifold base
345 (Qiagen) connected to the vacuum and eluted into 96-well PCR plates using 86 µL of 0.1 M
346 glycine-HCL buffer pH 2.7. After neutralization with 14 µL of 1 M Tris-HCl pH 8.0, purified
347 antibodies were buffer-exchanged into PBS using Zeba Spin Desalting Plates (Thermo Fisher
348 Scientific) and stored at 4°C until use.

349

350 **ELISA**

351 To assess antibody binding, soluble protein was plated at 2 µg/mL overnight at 4°C. The next
352 day, plates were washed three times with PBS supplemented with 0.05% Tween-20 (PBS-T)
353 and coated with 5% milk powder in PBS-T. Plates were incubated for one hour at room

354 temperature and then washed three times with PBS-T. Primary antibodies were diluted in 1%
355 milk in PBS-T, starting at 10 μg/mL with a serial 1:5 dilution and then added to the plate. The
356 plates were incubated at room temperature for one hour and then washed three times in PBS-T.
357 The secondary antibody, goat anti-human IgG conjugated to peroxidase, was added at 1:10,000
358 dilution in 1% milk in PBS-T to the plates, which were incubated for one hour at room
359 temperature. Plates were washed three times with PBS-T and then developed by adding TMB
360 substrate to each well. The plates were incubated at room temperature for ten minutes, and
361 then 1N sulfuric acid was added to stop the reaction. Plates were read at 450 nm.
362 Data are represented as mean ± SEM for one ELISA experiment. ELISAs were repeated 2 or
363 more times. If ELISA replicates were inconsistent over more than three experiments, antibody
364 was excluded from in vitro characterization analysis. The area under the curve (AUC) was
365 calculated using Prism software version 8.0.0 (GraphPad).
366
367 **ACE2 Binding Inhibition Assay**
368 96-well plates were coated with 2 μg/mL purified recombinant SARS-CoV-2 at 4°C overnight.
369 The next day, plates were washed three times with PBS supplemented with 0.05% Tween-20
370 (PBS-T) and coated with 5% milk powder in PBS-T. Plates were incubated for one hour at room
371 temperature and then washed three times with PBS-T. Purified anti were diluted in blocking
372 buffer at 10 μg/mL in triplicate, added to the wells, and incubated at room temperature. Without
373 washing, recombinant human ACE2 protein with a mouse Fc tag was added to wells for a final
374 0.4 μg/mL concentration of ACE2 and incubated for 40 minutes at room temperature. Plates
375 were washed three times with PBS-T, and bound ACE2 was detected using HRP-conjugated
376 anti-mouse Fc antibody and TMB substrate. The plates were incubated at room temperature for
377 ten minutes, and then 1N sulfuric acid was added to stop the reaction. Plates were read at 450
378 nm. ACE2 binding without antibody served as a control. Experiment was done in biological
379 replicate and technical triplicates.

380

381 **BioLayer Interferometry (BLI)**

382 Purified antibodies were immobilized to AHC sensortips (FortéBio) to a response level of
383 approximately 1.4 nm in a buffer composed of 10 mM HEPES pH 7.5, 150 mM NaCl, 3 mM
384 EDTA, 0.05% Tween 20 and 0.1% (w/v) BSA. Immobilized antibodies were then dipped into
385 wells containing two-fold dilutions of either SARS-CoV-2 RBD-SD1 (residues 306–577) or
386 SARS-CoV-2 NTD, ranging in concentration from 10–0.156 nM, to measure association
387 kinetics. Dissociation kinetics were measured by dipping sensortips into wells containing only
388 buffer. Data were reference subtracted and kinetics were calculated in Octet Data Analysis
389 software v10.0 using a 1:1 binding model.

390

391 **RTCA Method for Initial Screening of Antibody Neutralizing Activity**

392 To screen for neutralizing activity in the panel of recombinantly expressed antibodies, we used a
393 high-throughput and quantitative RTCA assay and xCelligence RTCA HT Analyzer (ACEA
394 Biosciences) that assesses kinetic changes in cell physiology, including virus-induced
395 cytopathic effect (CPE). Twenty µL of cell culture medium (DMEM supplemented with 2% FBS)
396 was added to each well of a 384-well E-plate using a ViaFlo384 liquid handler (Integra
397 Biosciences) to obtain background reading. Six thousand (6,000) Vero-furin cells in 20 µL of cell
398 culture medium were seeded per well, and the plate was placed on the analyzer. Sensograms
399 were visualized using RTCA HT software version 1.0.1 (ACEA Biosciences). For a screening
400 neutralization assay, equal amounts of virus were mixed with micro-scale purified antibodies in
401 a total volume of 40 µL using DMEM supplemented with 2% FBS as a diluent and incubated for
402 1 h at 37°C in 5% CO_2. At ~17–20 h after seeding the cells, the virus–antibody mixtures were
403 added to the cells in 384-well E-plates. Wells containing virus only (in the absence of antibody)
404 and wells containing only Vero cells in medium were included as controls. Plates were
405 measured every 8–12 h for 48–72 h to assess virus neutralization. Micro-scale antibodies were

406 assessed in four 5-fold dilutions (starting from a 1:20 sample dilution), and their concentrations
407 were not normalized. Neutralization was calculated as the percent of maximal cell index in
408 control wells without virus minus cell index in control (virus-only) wells that exhibited maximal
409 CPE at 40–48 h after applying virus–antibody mixture to the cells. An antibody was classified as
410 fully neutralizing if it completely inhibited SARS-CoV-2-induced CPE at the highest tested
411 concentration, while an antibody was classified as partially neutralizing if it delayed but did not
412 fully prevent CPE at the highest tested concentration[2, 22].
413
414 **Real-time Cell Analysis (RTCA) Neutralization Assay**
415 To determine neutralizing activity of IgG, we used real-time cell analysis (RTCA) assay on an
416 xCELLigence RTCA MP Analyzer (ACEA Biosciences Inc.) that measures virus-
417 induced cytopathic effect (CPE)[23]. Briefly, 50 µL of cell culture medium (DMEM supplemented
418 with 2% FBS) was added to each well of a 96-well E-plate using a ViaFlo384 liquid handler
419 (Integra Biosciences) to obtain background reading. A suspension of 18,000 Vero-E6 cells in
420 50 µL of cell culture medium was seeded in each well, and the plate was placed on the
421 analyzer. Measurements were taken automatically every 15 min, and the sensograms were
422 visualized using RTCA software version 2.1.0 (ACEA Biosciences Inc). VSV-SARS-CoV-2 (0.01
423 MOI, ~120 PFU per well) was mixed 1:1 with a dilution of antibody in a total volume of 100 µL
424 using DMEM supplemented with 2% FBS as a diluent and incubated for 1 h at 37°C in 5% CO_2.
425 At 16 h after seeding the cells, the virus-antibody mixtures were added in replicates to the cells
426 in 96-well E-plates. Triplicate wells containing virus only (maximal CPE in the absence of
427 antibody) and wells containing only Vero cells in medium (no-CPE wells) were included as
428 controls. Plates were measured continuously (every 15 min) for 48 h to assess virus
429 neutralization. Normalized cellular index (CI) values at the endpoint (48 h after incubation with
430 the virus) were determined using the RTCA software version 2.1.0 (ACEA Biosciences Inc.).
431 Results are expressed as percent neutralization in a presence of respective antibody relative to

432 control wells with no CPE minus CI values from control wells with maximum CPE. RTCA
433 IC_{50} values were determined by nonlinear regression analysis using Prism software.
434
435 **Plaque Reduction Neutralization Test (PRNT)**
436 The virus neutralization with live authentic SARS-CoV-2 virus (USA-WA1) was performed in the
437 BSL-3 facility of the Galveston National Laboratory using Vero E6 cells (ATCC CRL-1586)
438 following the standard procedure. Vero E6 cells were cultured in 96-well plates (10^4 cells/well).
439 Next day, 4-fold serial dilutions of antibodies were made using MEM-2% FBS, as to get an initial
440 concentration of 100 µg/mL. Equal volume of diluted antibodies (60 µL) were mixed gently with
441 original SARS-CoV-2 (USA-WA1) (60 µL containing 200 pfu) and incubated for 1 h at 37°C/5%
442 CO_2 atmosphere. The virus-serum mixture (100 µL) was added to cell monolayer in duplicates
443 and incubated for 1 at h 37°C/5% CO_2 atmosphere. Later, the virus-serum mixture was
444 discarded gently, and cell monolayer was overlaid with 0.6% methylcellulose and incubated for
445 2 days. The overlay was removed, and the plates were fixed in 4% paraformaldehyde twice
446 following BSL-3 protocol. The plates were stained with 1% crystal violet and virus-induced
447 plaques were counted. The percent neutralization and/or NT_{50} of antibody was calculated by
448 dividing the plaques counted at each dilution with plaques of virus-only control. For antibodies,
449 the inhibitory concentration at 50% (IC_{50}) values were calculated in Prism software (GraphPad)
450 by plotting the midway point between the upper and lower plateaus of the neutralization curve
451 among dilutions.
452
453 **Fab Preparation**
454 To generate Fabs, IgGs were incubated with Lys-C at 1:4,000 (weight:weight) overnight at
455 37 °C. EDTA free protease inhibitor (Roche) was dissolved to 25X and then added to the
456 sample at a final 1X concentration. The sample was passed over a Protein A column. The flow-

457 through was collected run on a Superdex 200 Increase 10/300 GL Sizing column on the AKTA
458 FPLC system. Fabs were visualized on SDS-PAGE.
459
460 **Electron Microscopy Sample Preparation and Data Collection**
461 Purified SARS-CoV-2 S HexaPro ectodomain[24] and Fabs 5317-4 and 5317-10 were combined
462 at a final complex concentration of 0.4 mg/mL. Fab 5317-10 was added to spike and incubated
463 on ice for 30 minutes before the addition of Fab 5317-4 immediately prior to grid deposition and
464 freezing. The complex was deposited on Au-300 1.2/1.3 grids that had been plasma cleaned for
465 4 minutes in a Solarus 950 plasma cleaner (Gatan) with a 4:1 ratio of O_2/H_2. Excess liquid was
466 blotted for 3 seconds with a force of -4 using a Vitrobot Mark IV (Thermo Fisher) and plunge
467 frozen into liquid ethane. 2,655 micrographs were collected from a single grid with the stage at a
468 30° tilt using a Titan Krios (Thermo Fisher) equipped with a K3 detector (Gatan). Movies were
469 collected using SerialEM[25] at 29,000X magnification with a corresponding calibrated pixel size
470 of 0.81 Å/ pixel.
471
472 **Cryogenic Electron Microscopy (Cryo-EM)**
473 Motion correction, CTF estimation, particle picking, and 2D classification were performed using
474 cryoSPARC v3.2.0[26]. The final iteration of 2D class averaging distributed 17,710 particles into
475 50 classes using an uncertainty factor of 3. From that, 13,232 particles were selected and an ab
476 inito reconstruction was performed with four classes followed by heterogeneous refinement of
477 those four classes. 6,803 particles from the highest-quality class were used for homogenous
478 refinement of the best volume without imposed symmetry. The resulting volume was used for an
479 additional round of homogenous refinement. To filter out additional junk particles, an *ab initio*
480 reconstruction was performed with three classes followed by heterogeneous refinement of those
481 three classes. 5,171 particles from the highest-quality class were used for homogenous
482 refinement of the best volume without imposed symmetry, resulting in a final 9 Å map.

483

484 **QUANTIFICATION AND STATISTICAL ANALYSIS**

485 ELISA error bars (standard error of the mean) were calculated using GraphPad Prism version
486 8.0.0. ANOVA analysis was performed for neutralization potency comparisons using GraphPad
487 Prism version 8.0.0.

488

489

490 **FIGURE CAPTIONS**

491

492 **Figure 1. Recovery of antibodies using LIBRA-seq with ligand blocking. A.** Experimental
493 setup of three LIBRA-seq experiments: experiment 1, LIBRA-seq with ligand blocking;
494 experiment 2, LIBRA-seq with a SARS-CoV-2 S titration; and experiment 3, LIBRA-seq with a
495 SARS-CoV-2 S titration and ligand blocking. After next-generation sequencing, hundreds of B
496 cells were recovered that had paired heavy/light chain sequencing information and antigen
497 reactivity information for the three experiments. For experiment 1 (**B**), 2 (**C**), and 3 (**D**), LIBRA-
498 seq scores for all cells per experiment are shown as open circles. Antibodies chosen for
499 expression and validation are highlighted in light blue. LIBRA-seq scores for antigens in each
500 experimental library for antibodies expressed are shown from -2 to 2, as tan to purple,
501 respectively. Scores outside of this range are shown as the minimum and maximum values. For
502 experiment 2 and 3, six different aliquots of S protein were added in a titration series (1-6).

503

504 **Figure 2. Validation and characterization of expressed antibodies.** Names of antibodies
505 that were expressed and their characteristics are shown. Each row represents an antibody. **A.**
506 ELISA area under the curve (AUC) values for binding to SARS-CoV-2 recombinant antigen
507 proteins and a negative control influenza hemagglutinin protein are shown for antibodies in each
508 experiment calculated from data in Supplementary Figure 2B. **B.** Affinity (K_D) of antibodies for
509 SARS-CoV-2 RBD or NTD (based on epitope shown in A) was determined by biolayer
510 interferometry. ND, not done. **C.** Percent reduction in ACE2 binding by ELISA is shown as a
511 heatmap from 0 to 100% reduction in binding as white to blue respectively. **D.** VSV SARS-CoV-
512 2 neutralization IC_{50} values are shown as a heatmap from high potency (red) to low potency
513 (green). Non-neutralizing antibodies are shown as white. For **E** and **F**, "Predicted Neutralizing
514 Antibodies" were defined as the subset of selected antibodies with low ACE2 LIBRA-seq scores
515 from experiments 1 and 3, and all antibodies with high LIBRA-seq scores for SARS-CoV-2 S

516 from experiment 2. **E.** For these predicted neutralizers, plotted are the IC_{50} values (μg/mL) for
517 SARS-CoV-2 neutralization by real time cell analysis (RTCA) with VSV-SARS-CoV-2 (IC_{50} value
518 for each antibody shown as single dot). Line shown is geometric mean. Non-neutralizing
519 antibodies are shown as >10 μg/mL. **F.** The percent of neutralizing antibodies from the set of
520 predicted neutralizers is shown for each experiment. **G.** Authentic SARS-CoV-2 neutralization
521 for a panel of antibodies is shown. IC_{50} values are shown to the right of the panel. **H.** 10 Å-
522 resolution cryo-EM structure of Fab-spike complex for 5317-4 Fab (orange) and 5317-10 Fab
523 (pink). Spike protomers are shown in green, blue, and red. **I.** Fab-spike complex structure
524 modeled with ACE2 (purple).
525
526 **Supplementary Figure 1. Set up of LIBRA-seq experiments.**
527 **A.** An antigen screening library of oligonucleotide-labeled antigens was generated. This library
528 consisted of SARS-CoV-2 spike antigens and negative controls. Additionally, oligo-labeled
529 ACE2 (the SARS-CoV-2 spike host cell receptor) was included. The antigen screening library
530 was mixed with donor PBMCs. This approach allowed for assessment of B cell ligand blocking
531 functionality from the sequencing experiment. **B.** We applied an antigen screening library
532 containing an antigen titration with a goal of identifying high affinity antibodies from LIBRA-seq.
533 In this experiment, six different amounts of oligo-labeled SARS-CoV-2 S protein, each labeled
534 with a different barcode, were included in a screening library, with the hypothesis that antibodies
535 with high affinity for SARS-CoV-2 S would show reactivity (high LIBRA-seq score) even with the
536 S protein added in lower amounts. **C**. Schematic of LIBRA-seq with S titrations and ACE2
537 included for ligand blocking.
538
539 **Supplementary Figure 2. Characterization of LIBRA-seq identified antibodies.**
540 **A.** Genetic characteristics for monoclonal antibodies prioritized for expression and validation.
541 V_H, J_H, V_L, J_L inferred gene segment identity is shown at the nucleotide level. CDRH3 and

542 CDRL3 amino acid sequence and length are shown. **B.** ELISA binding of antibodies to SARS-
543 CoV-2 spike, SARS-CoV spike, SARS-CoV-2 RBD, SARS-CoV-2 NTD, SARS-CoV-2 S2 and
544 influenza virus H1 NC99. ELISAs were performed in technical duplicates and repeated at least
545 two times. Data are represented as mean ± SEM. **C**. ACE2 blocking ELISA. Antibodies were
546 added to spike and recombinant ACE2 was added and detected. Antibodies that block ACE2
547 binding show a reduction in absorbance compared to ACE2 binding without competitor (dotted
548 line). ELISAs were performed at one antibody concentration in triplicate and were repeated at
549 least twice. Data are represented as mean ± SEM. **D.** Antibodies were tested in a VSV SARS-
550 CoV-2 RTCA neutralization assay. Neutralization curves and IC_{50} values are shown.
551

552 **References**

553 1. Jiang, S., Hillyer, C. & Du, L. Neutralizing Antibodies against SARS-CoV-2 and Other
554 Human Coronaviruses. *Trends Immunol* **41**, 355-359 (2020).
555 2. Zost, S.J. et al. Potently neutralizing and protective human antibodies against SARS-
556 CoV-2. *Nature* **584**, 443-449 (2020).
557 3. Chi, X. et al. A neutralizing human antibody binds to the N-terminal domain of the Spike
558 protein of SARS-CoV-2. *Science* **369**, 650-655 (2020).
559 4. Wec, A.Z. et al. Broad neutralization of SARS-related viruses by human monoclonal
560 antibodies. *Science* **369**, 731-736 (2020).
561 5. Brouwer, P.J.M. et al. Potent neutralizing antibodies from COVID-19 patients define
562 multiple targets of vulnerability. *Science* **369**, 643-650 (2020).
563 6. Rogers, T.F. et al. Isolation of potent SARS-CoV-2 neutralizing antibodies and protection
564 from disease in a small animal model. *Science* **369**, 956-963 (2020).
565 7. Hansen, J. et al. Studies in humanized mice and convalescent humans yield a SARS-
566 CoV-2 antibody cocktail. *Science* **369**, 1010-1014 (2020).

567 8. Krammer, F. SARS-CoV-2 vaccines in development. *Nature* **586**, 516-527 (2020).
568 9. Crowe, J.E., Jr. Principles of Broad and Potent Antiviral Human Antibodies: Insights for
569 Vaccine Design. *Cell Host Microbe* **22**, 193-206 (2017).
570 10. Scheid, J.F. et al. Broad diversity of neutralizing antibodies isolated from memory B cells
571 in HIV-infected individuals. *Nature* **458**, 636-640 (2009).
572 11. Wu, X. et al. Rational design of envelope identifies broadly neutralizing human
573 monoclonal antibodies to HIV-1. *Science* **329**, 856-861 (2010).
574 12. Busse, C.E., Czogiel, I., Braun, P., Arndt, P.F. & Wardemann, H. Single-cell based high-
575 throughput sequencing of full-length immunoglobulin heavy and light chain genes. *Eur J*
576 *Immunol* **44**, 597-603 (2014).
577 13. DeKosky, B.J. et al. High-throughput sequencing of the paired human immunoglobulin
578 heavy and light chain repertoire. *Nat Biotechnol* **31**, 166-169 (2013).
579 14. Tan, Y.C. et al. Barcode-enabled sequencing of plasmablast antibody repertoires in
580 rheumatoid arthritis. *Arthritis Rheumatol* **66**, 2706-2715 (2014).
581 15. Setliff, I. et al. High-Throughput Mapping of B Cell Receptor Sequences to Antigen
582 Specificity. *Cell* **179**, 1636-1646 e1615 (2019).
583 16. Shiakolas, A.R. et al. Cross-reactive coronavirus antibodies with diverse epitope
584 specificities and Fc effector functions. *Cell Rep Med*, 100313 (2021).
585 17. Chen, P. et al. SARS-CoV-2 Neutralizing Antibody LY-CoV555 in Outpatients with
586 Covid-19. *N Engl J Med* **384**, 229-237 (2021).
587 18. Cohen, M.S. Monoclonal Antibodies to Disrupt Progression of Early Covid-19 Infection.
588 *N Engl J Med* **384**, 289-291 (2021).
589 19. Weinreich, D.M. et al. REGN-COV2, a Neutralizing Antibody Cocktail, in Outpatients with
590 Covid-19. *N Engl J Med* **384**, 238-251 (2021).
591 20. Alamyar, E., Duroux, P., Lefranc, M.P. & Giudicelli, V. IMGT((R)) tools for the nucleotide
592 analysis of immunoglobulin (IG) and T cell receptor (TR) V-(D)-J repertoires,

593 polymorphisms, and IG mutations: IMGT/V-QUEST and IMGT/HighV-QUEST for NGS.
594 *Methods Mol Biol* **882**, 569-604 (2012).
595 21. Gupta, N.T. et al. Change-O: a toolkit for analyzing large-scale B cell immunoglobulin
596 repertoire sequencing data. *Bioinformatics* **31**, 3356-3358 (2015).
597 22. Gilchuk, P. et al. Integrated pipeline for the accelerated discovery of antiviral antibody
598 therapeutics. *Nat Biomed Eng* **4**, 1030-1043 (2020).
599 23. Suryadevara, N. et al. Neutralizing and protective human monoclonal antibodies
600 recognizing the N-terminal domain of the SARS-CoV-2 spike protein. *Cell* **184**, 2316-
601 2331 e2315 (2021).
602 24. Hsieh, C.L. et al. Structure-based design of prefusion-stabilized SARS-CoV-2 spikes.
603 *Science* **369**, 1501-1505 (2020).
604 25. Mastronarde, D.N. Automated electron microscope tomography using robust prediction
605 of specimen movements. *J Struct Biol* **152**, 36-51 (2005).
606 26. Punjani, A., Rubinstein, J.L., Fleet, D.J. & Brubaker, M.A. cryoSPARC: algorithms for
607 rapid unsupervised cryo-EM structure determination. *Nat Methods* **14**, 290-296 (2017).
608

Figure 1

A

Experiment 1: Ligand Blocking

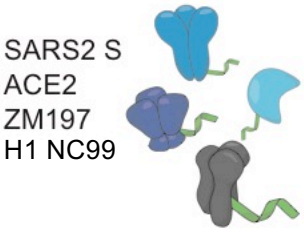

Experiment 2: SARS-CoV-2 S Titration

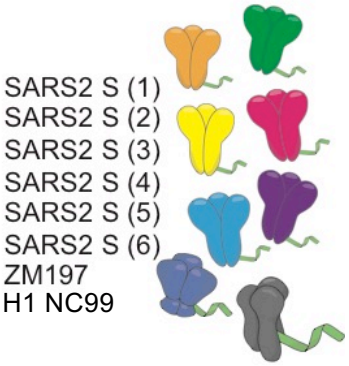

Experiment 3: SARS-CoV-2 S Titration + Ligand Blocking

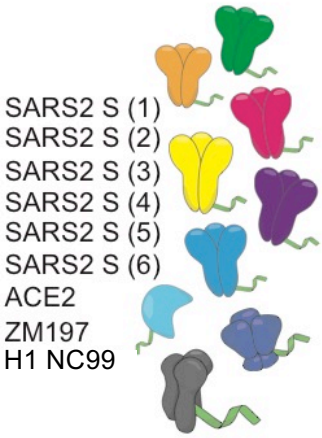

B

Experiment 1:Ligand Blocking

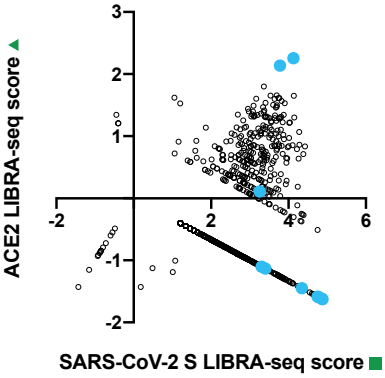

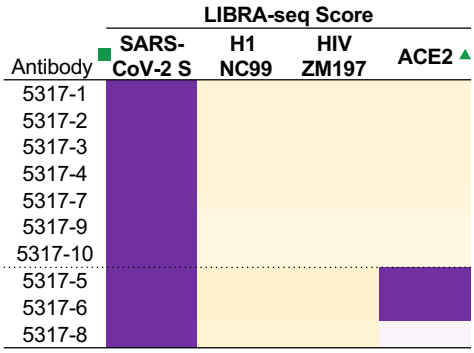

C

Experiment 2: SARS-CoV-2 S Titration

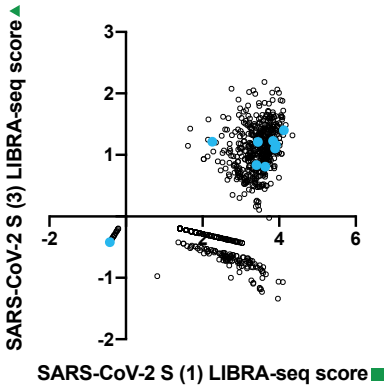

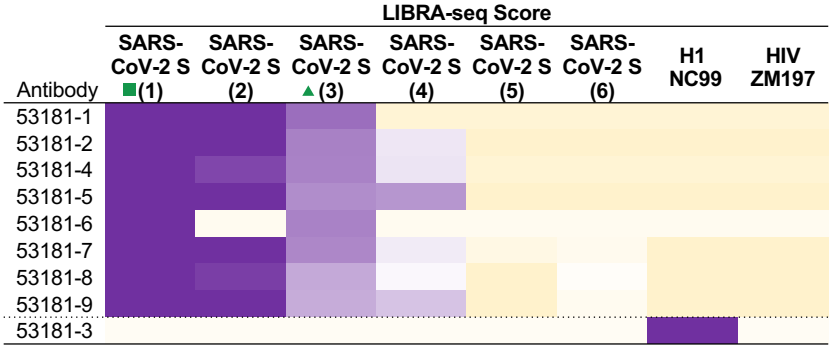

D

Experiment 3: SARS-CoV-2 S Titration + Ligand Blocking

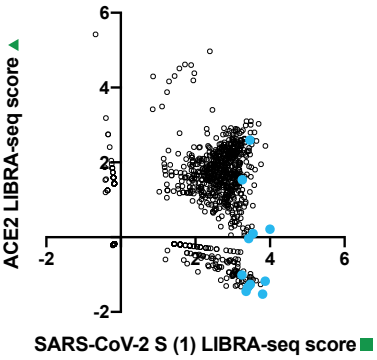

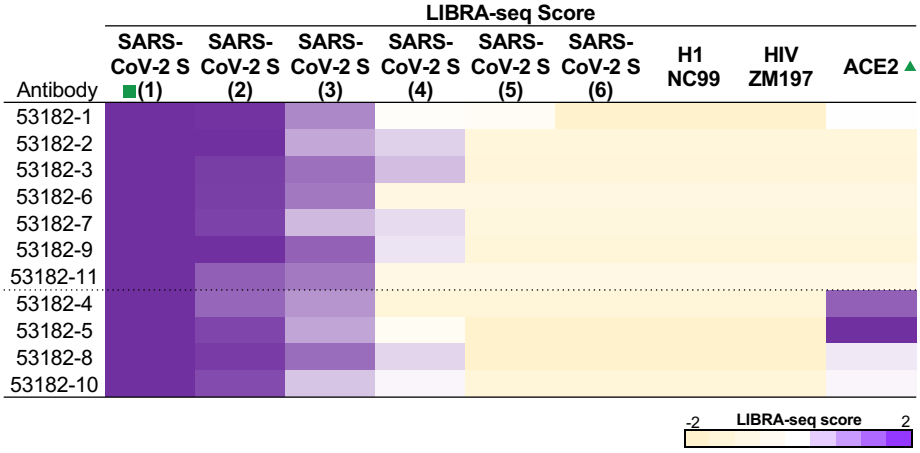

Figure 2

A

	Antibody	Binding Signal in ELISA (Area Under the Curve): SARS-CoV-2 S	SARS-CoV-2 S2	SARS-CoV-2 S1	SARS-CoV-2 RBD	SARS-CoV-2 NTD	H1 NC99	B: Affinity K_D (M)	C: % Reduction ACE2 Binding	D: Neut IC_{50} (µg/mL)
Experiment 1: Ligand Blocking	5317-1							4.34E-11	56	0.1218
	5317-2							1.95E-09	68	0.0829
	5317-3							1.92E-09	63	
	5317-4							1.78E-09	84	0.0148
	5317-7							1.05E-08	12	1.179
	5317-9							*ND*	-2	0.6326
	5317-10							*ND*	1	0.1816
	5317-5							8.26E-11	-3	
	5317-6							1.66E-09	0	
	5317-8							*ND*	-1	
Experiment 2: S Titration	53181-1							1.17E-09	-2	0.456
	53181-2							3.13E-08	-3	0.78
	53181-4							*ND*	0	
	53181-5							*ND*	-2	
	53181-7							*ND*	-1	
	53181-8							*ND*	-1	
	53181-9							*ND*	0	
	53181-3							*ND*	-1	
Experiment 3: S Titration + Ligand Blocking	53182-1							2.81E-09	84	0.343
	53182-3							8.32E-09	87	0.253
	53182-6							9.35E-10	91	0.077
	53182-7							2.15E-07	3	
	53182-9							4.75E-11	82	0.289
	53182-11							3.18E-09	7	
	53182-4							2.28E-09	0	
	53182-5							*ND*	-2	
	53182-8							1.65E-08	84	

ELISA AUC: min – max

% Reduction in Binding: 0 – 100

IC_{50} (µg/mL): 0.001 – 1 – 10

Non-neutralizing

E

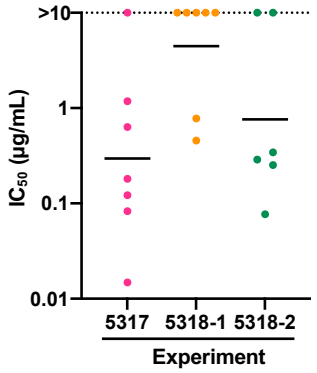

F

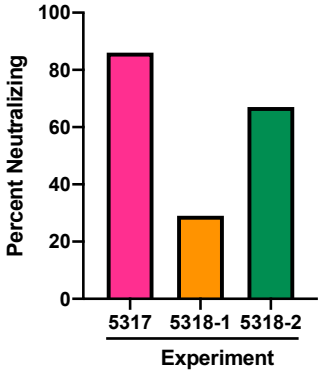

G

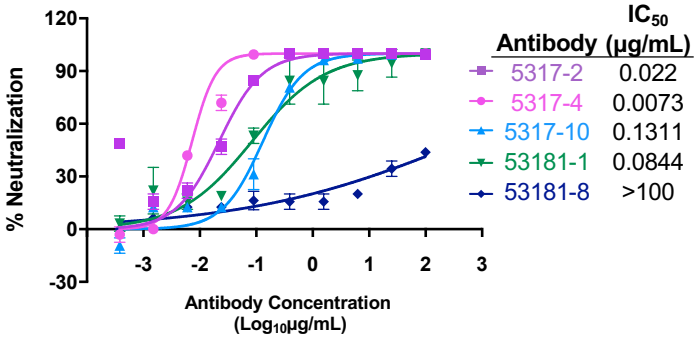

H

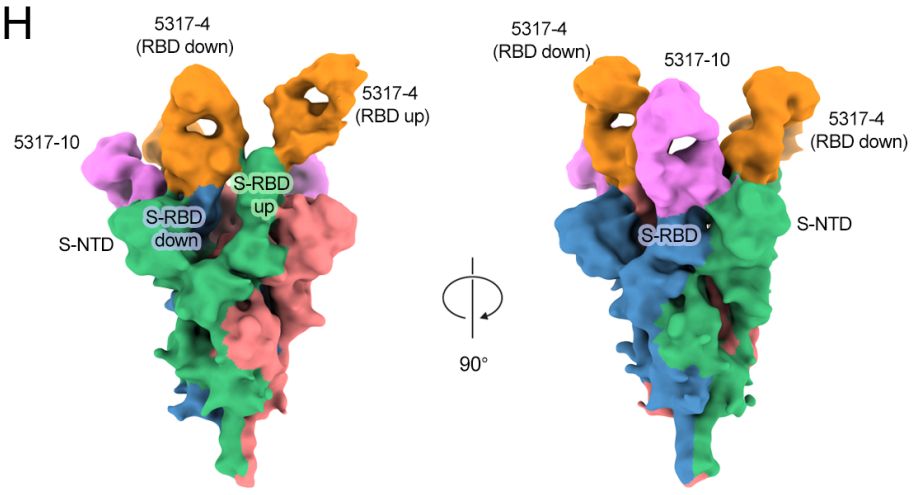

I

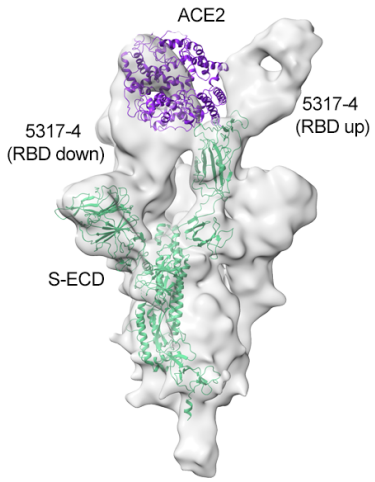

Supplementary Figure 1

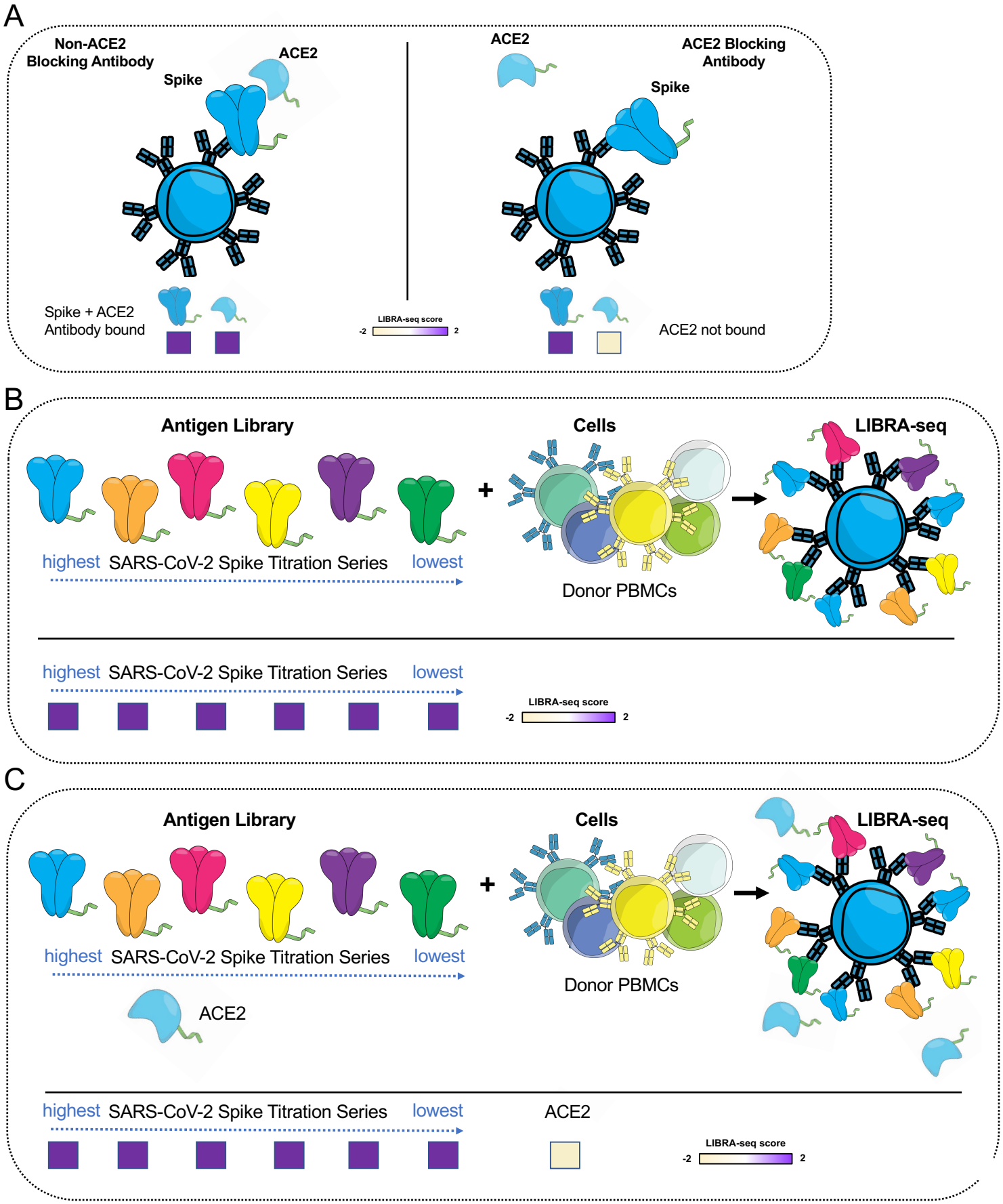

Supplementary Figure 2

A

Antibody	V^H Gene	J^H Gene	V^H Identity	J^H Identity	CDRH3 Sequence	CDRH3 Length	V^L Gene	J^L Gene	V^L Identity	J^L Identity	CDRL3 Sequence	CDRL3 Length
5317-1	*IGHV1-58*	*IGHJ4*	0.95	0.88	CAADPFADYW	8	*IGLV1-44*	*IGLJ3*	0.98	0.95	CATWDDSLNAWVF	11
5317-2	*IGHV1-69*	*IGHJ5*	0.95	0.92	CARGLWFGDSETVWFDPW	16	*IGKV1-39*	*IGKJ1*	0.97	0.97	CQQSYSTPPTF	9
5317-3	*IGHV3-64D*	*IGHJ4*	0.93	0.88	CVKGKIQLWLGADYW	13	*IGKV1-39*	*IGKJ1*	0.97	1.00	CQQSYNTPWTF	9
5317-4	*IGHV4-34*	*IGHJ3*	0.93	0.88	CARKPLLHSSVNPGAFDIW	17	*IGKV3-20*	*IGKJ2*	0.96	0.92	CQQYATSPRTF	9
5317-5	*IGHV1-69*	*IGHJ4*	0.97	0.96	CAREKGYSSSSSATYYLDFW	18	*IGLV1-40*	*IGLJ2*	0.98	0.95	CQSYDSSLTALVF	11
5317-6	*IGHV4-39*	*IGHJ6*	0.97	0.84	CARRVPGDYYCLDVW	13	*IGKV1-39*	*IGKJ4*	0.96	0.95	CQQSFSARVPTF	10
5317-7	*IGHV3-7*	*IGHJ4*	0.97	0.88	CARGGLWGTFDYW	11	*IGKV3-20*	*IGKJ2*	0.98	1.00	CQQFAYSLYTF	9
5317-8	*IGHV3-30-3*	*IGHJ6*	0.96	0.87	CARAYGGNYYYGMDVW	14	*IGLV3-1*	*IGLJ1*	0.96	0.97	CQAWDSSTASFVF	11
5317-9	*IGHV1-69*	*IGHJ5*	0.95	0.84	CASLGGDSYISGTHYDRSGYDPW	21	*IGKV3-11*	*IGKJ4*	0.98	0.95	CQRRSNWPPFTF	10
5317-10	*IGHV5-10-1*	*IGHJ4*	0.93	0.81	CARVNRVGDGPDFW	12	*IGKV2-28*	*IGKJ1*	0.97	1.00	CMQALQTPWTF	9
53181-1	*IGHV1-18*	*IGHJ6*	0.97	0.95	CARDPASYYDFWSGYVDYYYYGMDVW	24	*IGKV3-20*	*IGKJ3*	0.99	1.00	CQQYGNSRLTF	9
53181-2	*IGHV1-18*	*IGHJ6*	0.99	0.95	CARDPASYYDLWSGYVDYYYYGMDVW	24	*IGKV3-20*	*IGKJ3*	0.99	1.00	CHHYGSSRLTF	9
53181-3	*IGHV1-69*	*IGHJ4*	0.91	0.75	CARSGGYRLWFGELW	13	*IGKV3-20*	*IGKJ5*	0.94	0.95	CQQYGGSPATF	9
53181-4	*IGHV3-33*	*IGHJ4*	0.98	0.88	CAREGAVGATSGLDYW	14	*IGLV3-10*	*IGLJ3*	0.99	0.89	CYSRDSSGNPLF	10
53181-5	*IGHV4-59*	*IGHJ4*	0.95	0.96	CARGFDYW	6	*IGKV3-20*	*IGKJ1*	0.98	1.00	CQQYGSSPWTF	9
53181-6	*IGHV4-59*	*IGHJ6*	0.94	0.89	CARGAGEQRLVGGLFGVSHFYYYMDVW	25	*IGKV1-5*	*IGKJ1*	0.99	1.00	CQQYNSYPWTF	9
53181-7	*IGHV3-23*	*IGHJ4*	0.94	0.81	CAKSATIVLMVSAIYW	14	*IGLV2-14*	*IGLJ2*	0.97	1.00	CSSYTSTSTLVF	10
53181-8	*IGHV3-72*	*IGHJ6*	0.99	0.94	CARVRGGEWVGDLGWYYYYGMDVW	22	*IGKV2-28*	*IGKJ2*	0.99	0.97	CMQALQTPRTF	9
53181-9	*IGHV3-30*	*IGHJ4*	0.91	0.92	CVKGATKIDYW	9	*IGLV2-14*	*IGLJ1*	0.91	0.83	CFSYTSGGTRVF	10
53182-1	*IGHV3-53*	*IGHJ3*	0.95	0.96	CTRGGWPSGDTFDIW	13	*IGKV1-9*	*IGKJ3*	0.99	0.97	CQQLNSYPEITF	10
53182-2	*IGHV3-48*	*IGHJ5*	0.98	0.92	CAREGGWYSVGWVDPW	14	*IGKV3-20*	*IGKJ2*	0.98	0.97	CQQYGSSRTF	8
53182-3	*IGHV3-66*	*IGHJ6*	0.99	0.87	CARDRRIIGYYFGMDVW	15	*IGLV2-23*	*IGLJ3*	0.97	1.00	CCPYADTWVF	8
53182-4	*IGHV2-5*	*IGHJ3*	0.85	0.86	CARLLIEHDAFDIW	12	*IGKV2-28*	*IGKJ2*	0.92	0.97	CMQALHFPYTF	9
53182-5	*IGHV1-69*	*IGHJ4*	0.85	0.88	CAREEGSGWWKHDYW	13	*IGKV1-9*	*IGKJ2*	0.97	1.00	CQQLSGYPYTF	9
53182-6	*IGHV3-66*	*IGHJ6*	0.95	0.84	CVRDRRIVGYYFGLDVW	15	*IGLV2-23*	*IGLJ3*	0.96	0.95	CCSYATTWVF	8
53182-7	*IGHV3-23*	*IGHJ6*	0.98	0.97	CAKDAFYYGSGSHFYYYYYMDVW	21	*IGKV3-20*	*IGKJ5*	0.99	0.97	CQQYGSSPTF	8
53182-8	*IGHV4-39*	*IGHJ4*	0.99	0.92	CARDRRGGGWTASFDFW	15	*IGKV4-1*	*IGKJ2*	0.99	0.97	CQQHYSTPGYTF	10
53182-9	*IGHV3-53*	*IGHJ3*	0.98	0.98	CARGGWPSGDTFDIW	13	*IGKV1-9*	*IGKJ3*	0.99	0.97	CQQLNSYPEITF	10
53182-10	*IGHV2-5*	*IGHJ4*	0.98	0.83	CAHHTVPTIYDYW	11	*IGLV2-8*	*IGLJ3*	0.98	0.97	CSSYAGSNPLVF	10
53182-11	*IGHV3-9*	*IGHJ3*	0.93	0.92	CAKDIGRYDHYNIFGRVGGAFDIW	22	*IGKV1-33*	*IGKJ3*	0.95	0.94	CQHYDNLPRF	8

B

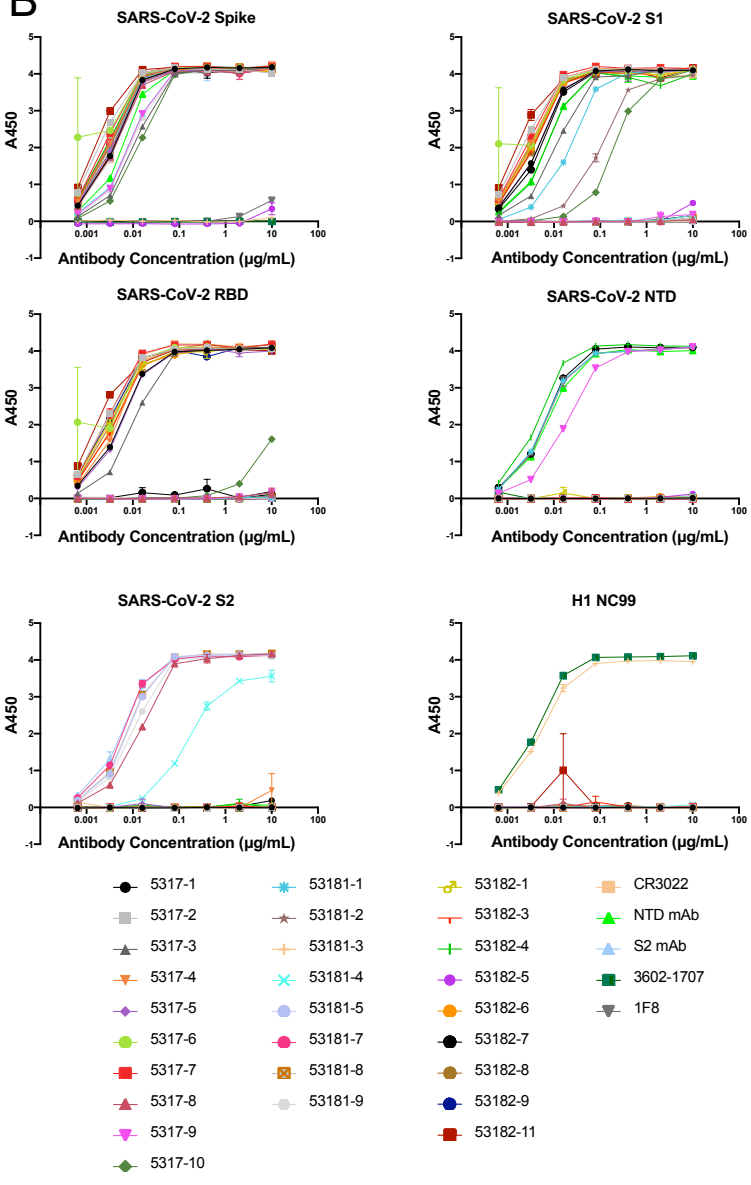

C

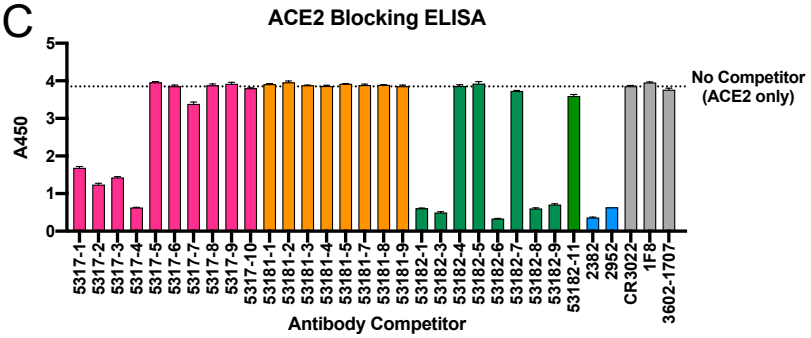
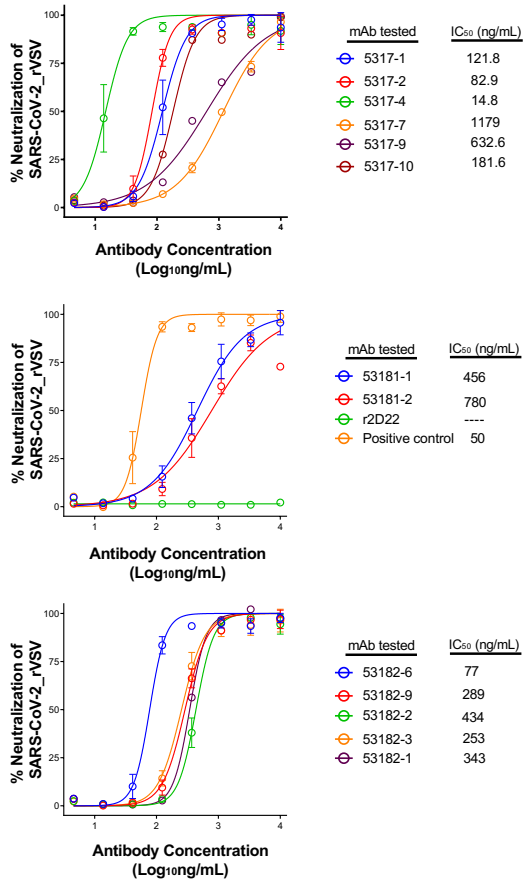
D